Journal of Hydroscience and Hydraulic Engineering
Vol. 17, No.1 May, 1999, 131-141

Numerical Analysis of Saline Intrusion with Propagation of Tide

By

Makoto Ifuku

and

Yoshihiro Kusu
Ehime University, Matsuyama Japan

SYNOPSIS

There have been few studies on salt wedge instability under the influence of tidal motion and the behavior of interfaces and interface instability conditions when tide propagates up rivers. To clarify these phenomena, it is necessary to carry out analysis with a vertical two-dimensional or three-dimensional numerical model. Further, the modeling of tide effects at the upstream boundary is an important issue. We carry out numerical analysis on the saline intrusion caused by propagation of tide, with two-dimensional Reynolds and diffusion equations used as the governing equations. It proves possible to explain the temporal variation of surface level as well as the vertical structure of flow and salinity during flood and ebb tides in the estuary. The location of isohalines changes periodically with variations in tide and depending upon the modified estuarine Richardson number proposed by Fischer.

INTRODUCTION

Estuaries are expanses of water connected to the sea at one end and fed by sources of fresh water (rivers) at their landward extremities. In such areas, saline sea-water and fresh river-water meet each other. As the salt and fresh waters mix, the distribution of salinity in the estuary is a gradually varying function of space and time.

Most of the mathematical models that have been developed to calculate the salinity distribution of estuaries are descriptive rather than predictive. A mathematical model offering predictive capabilities would require physical information on the spatial and temporal functions governing turbulent eddies and mass diffusivities as well as physically relevant boundary conditions of general applicability. However, our present knowledge of, for instance, the effect of stratification on vertical eddies and mass diffusivities is limited (Fischer(4)), and it is for this reason that current models tend to be descriptive rather than predictive.

A general representation of the salinity distribution in an estuary would require an unsteady, three-dimensional approach. For many situations, however, a simplified model may give satisfactory information in a much more economical way. For a lateral uniform situation, for instance, a vertical two-dimensional model is an obvious schematization.

There have been many studies on instability conditions at the interfaces during saltwater intrusion. However, most are experimental or theoretical investigations of the instability of shear flow and wind drift. There have been only a few studies on the instability of salt wedges under the influence of tidal motion, and of the behavior of interfaces and instability conditions at interfaces when tide propagates up rivers. Very recently, Komatsu et al.(5) investigated the characteristics of the several mixed types of turbulent shear flow and proposed a method of evaluating turbulent diffusivity, which is very important to clarify mixed saline intrusion.

To further elucidate these phenomena, it is necessary to use a two-dimensional, laterally integrated model or three-dimensional model for analysis. In addition, a very important question is how to evaluate the effects of tide propagation in river.

NUMERICAL ANALYSIS

Governing Equations

Flow

After integrating over the width of the channel and using the shallow water approximation, the equations for vertical two-dimensional density current can be outlined as below.

The equation for the conservation of longitudinal momentum reads

$$\frac{\partial u}{\partial t}+\frac{1}{B}\frac{\partial}{\partial x}(Bu^2)+\frac{\partial}{\partial z}(uw)=-\frac{1}{\rho}\frac{\partial p}{\partial x}+\frac{1}{\rho}\frac{1}{B}\frac{\partial}{\partial x}(B\tau_{xx})+\frac{1}{\rho}\frac{\partial \tau_{zx}}{\partial z} \tag{1}$$

where t = time; x = longitudinal coordinate (positive upstream); z = vertical coordinate (positive upward); u, w = longitudinal and vertical velocities, respectively; ρ = density; p = pressure; and B = channel width, which is assumed to be afunction of x only.

Moreover, τ_{xx} and τ_{zx} are the Reynolds stresses and are expressed in the notation of Cartesian tensors as follows

$$\left.\begin{aligned}&\tau_{ji}/\rho=(\nu+\nu_t)\left(\frac{\partial u_i}{\partial x_j}+\frac{\partial u_j}{\partial x_i}\right)\\&\nu_t=(c_s\Delta)^2\left[\left(\frac{\partial u_i}{\partial x_j}+\frac{\partial u_j}{\partial x_i}\right)\frac{\partial u_i}{\partial x_j}\right]^{1/2}\end{aligned}\right\} \tag{2}$$

where ν = kinematic viscosity; ν_t = SGS (subgrid-scale) diffusivity suggested by Smagorinsky(7); c_s = Smagorinsky constant; and $\Delta=(\Delta x\Delta z)^{1/3}$(with Δx and Δz the londitudinal and vertical grid intervals, respectively).

If the shallow water approximation is adapted, the equation for the conservation of vertical momentum reduces to the hydrostatic pressure distribution:

$$\frac{\partial p}{\partial z}=-\rho g \tag{3}$$

where g = gravitational acceleration. Integration of eq.(3) with respect to z yields the equation for pressure

$$\left.\begin{aligned}&p=\rho_0 g(\xi-z)+\beta g\textstyle\int_{z_b}^{\xi}S\,dz\\&\beta=\rho_0(\rho_s-\rho_0)/\rho_s\\&\rho=\rho_0+\beta S\end{aligned}\right\} \tag{4}$$

where ξ = position of the free water surface; z_b = z-coordinate of the bottom; ρ_0, ρ_s = density of fresh and salt waters, respectively; and S = salinity.

The continuity equation reads

$$\frac{1}{B}\frac{\partial(Bu)}{\partial x}+\frac{\partial w}{\partial z}=0 \tag{5}$$

Integration of eq.(5) over the water depth and substituting the kinematic boundary condition yields

$$\frac{\partial \xi}{\partial t}+\frac{1}{B}\frac{\partial}{\partial x}\left(B\int_{z_b}^{\xi}u\,dz\right)=0 \tag{6}$$

Salt Content

The equation for conservation of salt content reads

$$\frac{\partial S}{\partial t}+\frac{1}{B}\frac{\partial}{\partial x}(BuS)+\frac{\partial}{\partial z}(wS)=\frac{1}{B}\frac{\partial}{\partial x}\left(BK_{xx}\frac{\partial S}{\partial x}\right)+\frac{\partial}{\partial z}\left(K_{zz}\frac{\partial S}{\partial z}\right) \tag{7}$$

where K_{xx}, K_{zz} = turbulent diffusivities and are assumed to be as follows(Bear(1)):

$$\left.\begin{aligned}&K_{xx}=\gamma_x(a_L u^2+a_T w^2)/q\\&K_{zz}=\gamma_z(a_T u^2+a_L w^2)/q\\&q=(u^2+w^2)^{1/2}\end{aligned}\right\} \tag{8}$$

where γ_x, γ_z = constants of proportionality; and a_T, a_L=characteristic lengths defined as follows.

$$a_T = \Delta \; ; \; a_L = c_1 \cdot a_T \tag{9}$$

where c_1 = empirical constant.

Boundary Conditions (Fig.1)

The mathematical model requires boundary conditions and initial conditions for both the tidal motion and the salinity. The designation of the model as either descriptive or predictive depends on the formulation of the vertical momentum and mass exchange and on the way in which the boundary conditions are treated. If measured data are used and if they cannot be predicted in way that the vertical tidal motion at the sea can be predicted, the model is only descriptive.

Free Surface Boundary

At the water surface $z = \xi$, the conditions are:

$$\left.\begin{aligned} &\partial u/\partial z = 0 \\ &w_\xi S - K_{zz}(\partial S/\partial z) = 0 \end{aligned}\right\} \tag{10}$$

where w_ξ = vertical velocity at the water surface.

Bottom Boundary

At the bottom $z = z_b$, the conditions are:

$$\left.\begin{aligned} &u = 0, \;\; w = 0 \;\; \text{(nonslip)} \\ &\partial u/\partial z = 0, \; w_{z_b} = u_{z_b}\partial z_b/\partial x \;\; \text{(slip)} \\ &\partial S/\partial z = 0 \end{aligned}\right\} \tag{11}$$

Seaward Boundary

At the seaward boundary, the surface elevation, η, and the position of free surface water, ξ, must be specified

$$\left.\begin{aligned} &\eta(t) = a\sin\sigma t \\ &\xi(t) = h + \eta(t) \end{aligned}\right\} \tag{12}$$

where h = still water depth; a = tidal amplitude; σ = angular frequency ($\sigma = 2\pi/T$; T : the tidal period). Further, a boundary condition for longitudinal velocity must be imposed. Because in general no velocity profiles are available during the tidal cycle, a weak condition is imposed:

$$\partial^2 u/\partial x^2 = 0 \tag{13}$$

Finally a condition for the conservation of salt content must be given. During the flood tide, the increase in concentration is specified as a function of t and z. During the ebb tide, a weak condition is imposed, analogous to the condition for longitudinal velocity.

$$\left.\begin{aligned} &S = S_0 G(z,t) \quad u(z) \geq 0 \\ &G(z,t) \equiv (1 - S') + S'\sin\sigma t \\ &\partial^2 S/\partial x^2 = 0 \quad u(z) < 0 \end{aligned}\right\} \tag{14}$$

where S_0 = salinity of the sea and S' = coefficient. The form of $G(z,t)$ is one of the subjects of this investigation, and as a first approach a piece-wise linearized function of t, independent of z, was tried.

Upstream Boundary

If the river discharge is known and a logarithmic velocity profile is assumed for the river water region of the estuary, the only restriction on this boundary condition is that it must be broad enough to be outside the zone of salinity intrusion.

$$\left.\begin{aligned} &u = u_\xi \left[\ln\left\{\frac{(e-1)}{(\xi - z_b)}(z - z_b) + 1\right\}\right] \\ &S = 0 \end{aligned}\right\} \tag{15}$$

where u_ξ = velocity at the water surface. The velocity at the water surface, u_ξ, is evaluated using the following schemes:

(i)The water level and depth-averaged velocity, $\bar{u}_s$, are calculated using the shallow water equation.

(ii)The first relation in eq.(15) is averaged over the water depth. As a result, the relationship between u_ξ and the depth-averaged velocity, $\bar{u}$, is obtained. Now, it is assumed that $\bar{u}_s$ is equal to $\bar{u}$, and the velocity at the water surface is given, so the velocity profile can be determined.

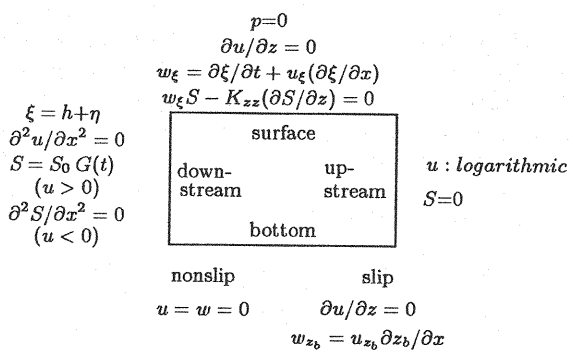

Fig.1 Boundary conditions

Coordinate Transformation

In the physical domain, the water surface is a moving boundary because of tide, and the bottom also changes in space.

$$\xi = \xi(x,t); \quad z_b = z(x,t) \tag{16}$$

Further, the longitudinal area of interest will not in general be a rectangle, because of variations in the bottom and the free surface. To obtain a good representation of the flow, a good description of the form of the free surface and the bottom is necessary. For a numerical approach based on finite differences, however, a rectangular grid that is coincident with the boundaries is preferable. Therefore, the area of interest is modified by a simple transformation into a rectangle (Fig.2).

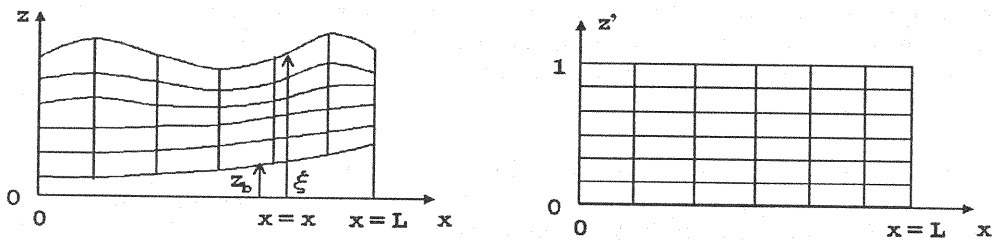

(a) Physical domain (b) Computational domain

Fig.2 Physical and computational domains

The relationship between the physical domain (x, z, t) and the computational domain (x, z', t) is expressed as follows.

$$\left.\begin{aligned} z' &= (z - z_b) f_b(x,t) \\ f_b(x,t) &\equiv 1/[\xi(x,t) - z_b(x,t)] \end{aligned}\right\} \tag{17}$$

$$\left.\begin{aligned} \partial/\partial t &= \partial/\partial t + F_1 \cdot \partial/\partial z' \\ \partial/\partial x &= \partial/\partial x + F_2 \cdot \partial/\partial z' \\ \partial/\partial z &= F_3 \cdot \partial/\partial z' \end{aligned}\right\} \tag{18}$$

Moreover, F_1, F_2, and F_3 are expressed as follows.

$$\left.\begin{aligned} F_1 &\equiv z'/f_b(\partial f_b/\partial t) - f_b(\partial z_b/\partial t) \\ F_2 &\equiv z'/f_b(\partial f_b/\partial x) - f_b(\partial z_b/\partial x) \\ F_3 &\equiv f_b \end{aligned}\right\} \tag{19}$$

The prescribed coordinate transformation is applied to the governing equations, and the spatial and temporal behavior of flow and salinity are then simulated.

NUMERICAL RESULTS

Analysis based on experiment by Perrels·Karelse(6)

The results of a flume test conducted by Perrels·Kareles were used to verify the numerical model. It was assumed that there was no density difference between river water and sea water. At the downstream boundary, the surface elevation was computed by the Airy wave theory with a wave amplitude of 2.5 cm and a period of 558.7 s. The river discharge was set at $2.9\text{x}10^{-3}$ m^3/s at the upstream boundary. The length, width, and depth of channel were 101.5 m, 0.672 m, and 0.216 m, respectively. A no-slip condition was imposed at the bottom. The horizontal grid interval was set to 1.83 m and the water depth was divided into 13 planes. The time increment was $T/1000$. The Smagorinsky constant in eq.(2) was set to 0.12.

Temporal variation in surface elevation

Figure 3 shows the temporal variation of surface elevation at points 3.66 m and 47.58 m from the river mouth. In this figure, the solid circles and the solid line represent the experimental and simulated results, respectively. There is a slight difference in surface elevation at the wave crest in (a), where x = 3.66 m, but there is no phase difference between the experimental and simulated results; the temporal variations are almost the same. In Fig.3(b), with x = 47.58 m, the experimental and simulated results exhibit a phase difference at both wave crest and trough. In the wave trough, the simulated water level is about 0.5 cm lower than the experimental value.

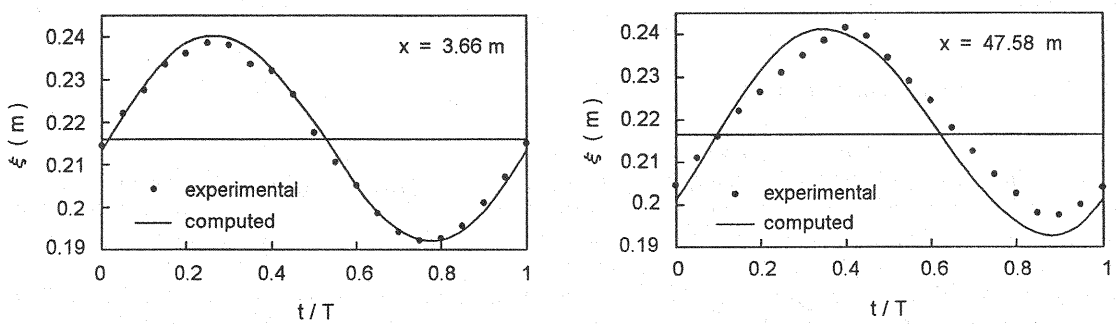

(a) x=3.66 m (b) x=47.58 m

Fig.3 Temporal variation in water level

Vertical distribution of horizontal velocity

Figure 4 shows the vertical distribution of horizontal velocity at points x = 10.98 m and x = 47.58 m for the phases at which the velocity reaches a maximum (referred as to MFV) and minimum (referred as to MEV) in the slack phase. The solid and open circles represent the experimental and simulated results, respectively.

Figure 4(a) shows the vertical distribution at point x = 10.98 m at MEV. The simulated velocity is slightly lower than the experimental value near the bottom and at the surface, while it is slightly larger at the intermediate depths. However, the difference between the experimental and simulated results is very small. Figure 4(b) shows the vertical distribution at point x = 47.58 m at MEV; these results are similar to that in Figure 4(a), both qualitatively and quantitatively. Figure 4(c) shows the vertical distribution at point x = 10.98 m at MFV. Here, the simulated velocity is slightly lower than the measured value at intermediate depths. Figure 4(d) shows the vertical distribution at point x = 47.58 m at MFV. The

simulated result is slightly greater. Overall, the differences between experimental and simulated results are very small. These results demonstrate that this numerical model is able to explain the vertical distribution of horizontal velocity with propagation of tide.

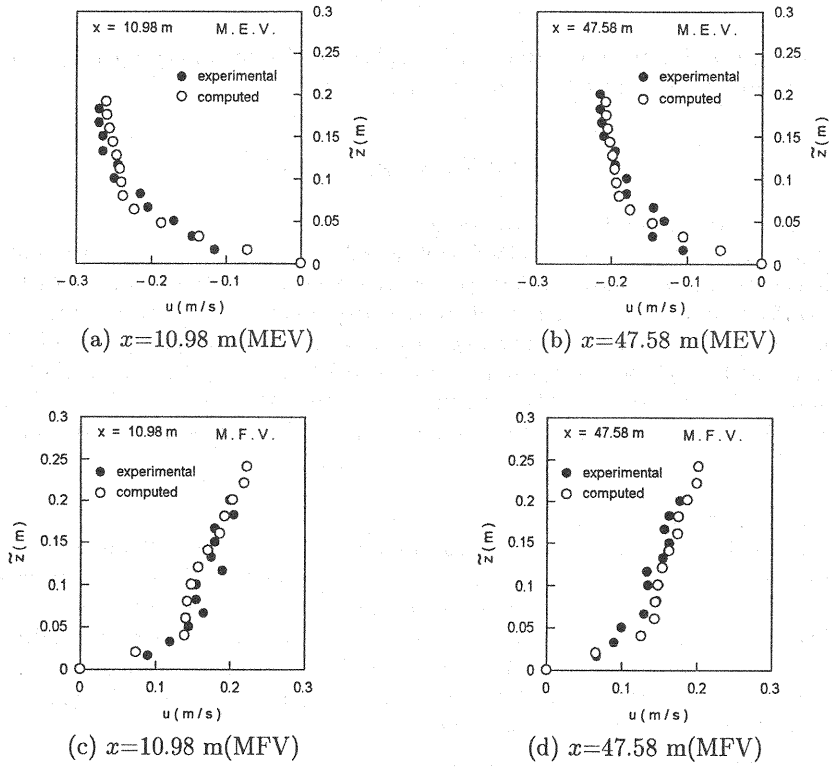

(a) x=10.98 m(MEV) (b) x=47.58 m(MEV)

(c) x=10.98 m(MFV) (d) x=47.58 m(MFV)

Fig.4 Vertical distribution of horizontal velocity

Analysis based on experiment by Komatsu et al.

The results of a flume test by Komatsu et al.(5) were also used for the verification of the numerical model. The salinity at the sea boundary was about 1 ‰. At the sea boundary, the surface elevation was computed by the Airy wave theory for wave amplitudes of 0.5, 0.65, 0.85, 1.2, 1.5, and 2 cm and a period of 240 s. Meanwhile, the river discharge was set at $3.5\text{x}10^{-5}$ m^3/s at the upstream boundary. The length and width of the channel were 20 m and 0.25 m, respectively, and the water depth at the sea boundary was 0.133 m. The bottom slope was 0.005 and an artificial roughness was provided with 1x1x25 cm blocks attached to the bottom at 0.1 m intervals. The horizontal grid interval was set to 0.05 m and the water depth was divided into 11 planes. The time increment was $T/1000$. The Smagorinsky constant in eq.(2) was set to 0.12. The constant of proportionality,γ_x, in eq.(8) and the empirical constant, c_1, in eq.(9) were set to 0.001 and 100, respectively. The values of the several constants used in this analysis are given in Table 1.

Table 1 Values of constants used in this analysis

a(cm)	c_1	γ_x	γ_z
0.5	100	0.001	0.003
0.6 - 1.2	100	0.001	0.01
1.5, 2	100	0.001	0.015

Temporal variation of surface elevation and salinity

Figure 5 shows the temporal variations of water level and salinity at point $x = 1$ m for a river water discharge of $3.5\text{x}10^{-5}$ m^3/s. The solid line represents water level. Near the bottom and at two-fifths of the water depth, salinity increases gradually with increasing water level. Once the water level passes its maximum, the salinity remains almost constant for a while; at a point $\pi/10$ radians after the tidal crest, the salinity at these planes is a maximum. Meanwhile, at the point $\pi/5$ radians ahead of the tidal crest, the salinity near the water surface is a maximum, thereafter remaining almost constant for a quarter of the tidal period. The salinity near the bottom reaches minimum at the tidal trough.

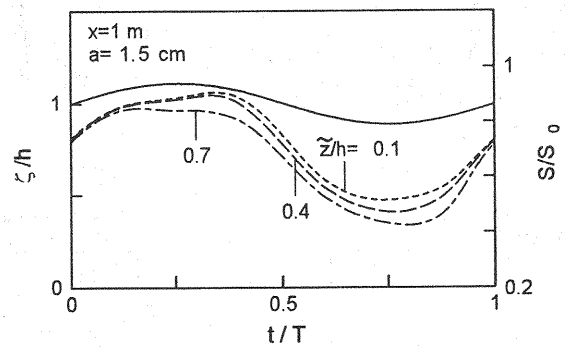

Fig.5 Temporal variation of water level and salinity

Surface elevation and non-dimensional turbulent diffusivity

Figure 6 shows the temporal variation of water level and non-dimensional turbulent diffusivity, $\tilde{K}_{xx}(\tilde{K}_{xx}=K_{xx}/\sqrt{gh^3})$, at point $x = 1$ m. The river water discharge was $3.5\text{x}10^{-5}$ m^3/s. The turbulent diffusivity is maximized during the slack tide. Comparing Fig.5 with Fig.6 shows that the phase in which the salinity peaks agrees with the phase in which the turbulent diffusivity is approximately zero. The reason for this is that the intrusion of salt water due to advection and diffusion phenomena comes to a halt when the velocity is zero, since these phenomena arise from turbulent diffusion which depends on velocity. Thereafter, the effect of river water discharge gradually becomes stronger and the salt water retreats.

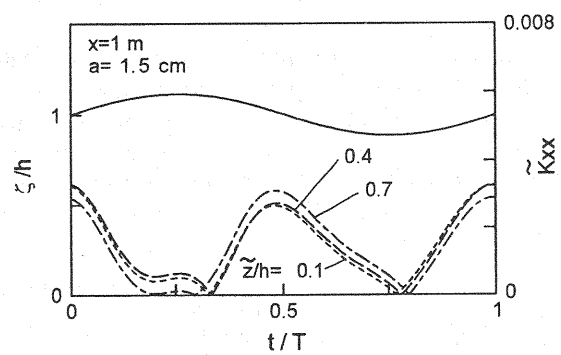

Fig.6 Temporal variation of water level and diffusivity

Vertical distribution of salinity

Figure 7 shows the vertical distribution of salinity at points $x = 3$ m and $x = 7$ m. Figures 7(a), (b) and Figs.7(c), (d) depict the distribution where non-slip and slip boundary conditions are imposed on the bottom, respectively. The solid and open circles, squares, and triangles depict experimental and simulated results for the flood, slack, and ebb phases, respectively.

Figure 7(a) shows that simulated results are larger than the experimental ones for velocity gradient near the bottom during flood and ebb tides. As shown in Fig.7(b), the simulated results agree well with the experimental ones during flood tide. However, the simulated results are larger than experimental ones at ebb and slack tides. Meanwhile, as shown in Figures 7(c) and 7(d), on the whole, the simulated results agree well with experimental ones during ebb and slack tides. Comparing Fig.7(c) with Fig.7(a),

the difference between simulated and experimental results is small when the slip condition is imposed.

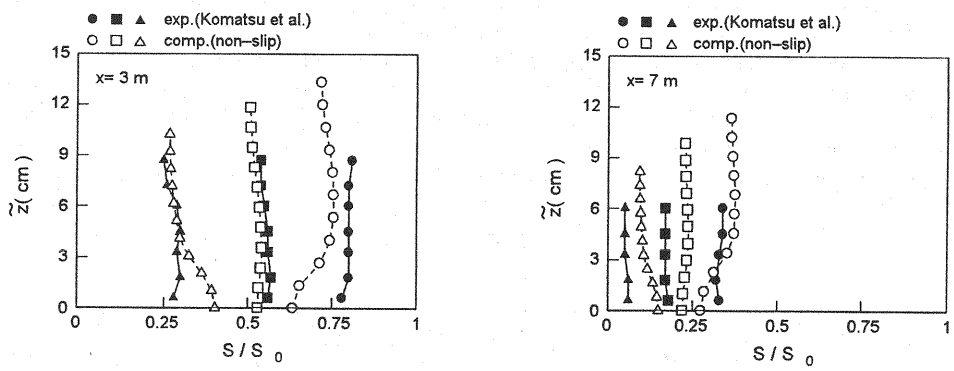

(a) x=3 m (non-slip) (b) x=7 m (non-slip)

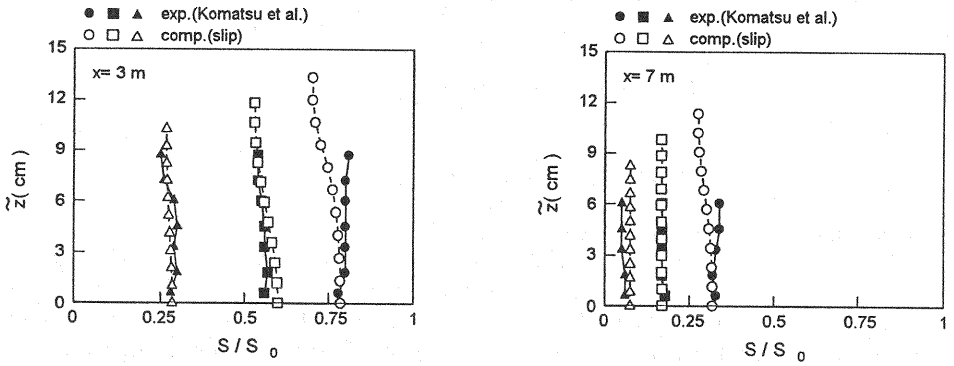

(c) x=3 m (slip) (d) x=7 m (slip)

Fig.7 Vertical distribution of salinity (a = 1.5 cm)

Spatial distribution of salinity averaged over water depth

Figure 8 shows the spatial distribution of salinity averaged over water depth. The solid and broken lines represent the simulated results when the slip condition is imposed at the bottom. The cases with amplitudes 0.5, 0.85, and 1.5 cm correspond to the salt wedge, partially mixed, and well-mixed types, respectively. In these three types, the simulated results reflect the experimental ones, although there is a slight difference between the two. Judging from these various results, the numerical model for saline intrusion is capable of predicting several types of saline intrusion with high accuracy.

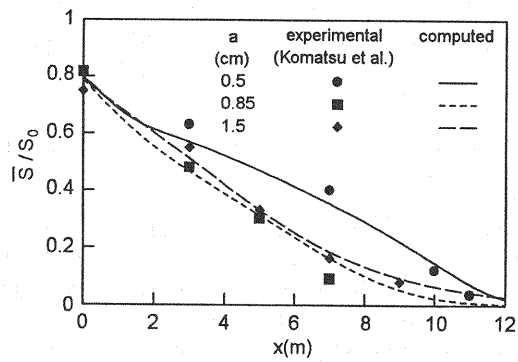

Fig.8 Spatial distribution of salinity averaged over water depth

Saline intrusion distance

Figure 9 shows the effect of the tidal amplitude and river discharge on saline intrusion distance,

L_s. Saline intrusion distance from the river mouth is defined as the position of the isohaline whose value is equal to 0.01 at the bottom. The river may be thought of as a source of deficit of potential energy, and the tide as a source of kinematic energy that overcomes the deficit. Taking this approach, Fischer(3) defined a modified estuarine Richardson number in an analogy with the "Pipe Richardson Number" defined by Ellison and Turner(2). The modified estuarine Richardson number, R^*_{iE}, is given by the following equation.

$$R^*_{iE} = s g Q / B u_*{}^3 \tag{20}$$

where s = relative difference density between the river and sea waters; $s = (\rho_s - \rho_0)/\rho_0$; u_* = r.m.s. of shear velocity; and Q = river water discharge at the upstream boundary.

The saline intrusion distance changes periodically with variations in tide and depends on the modified estuarine Richardson number. In a well-mixed estuary where the tidal amplitude is relatively large ($R^*_{iE} \simeq 7$), the intrusion distance is a maximum, and it is also relatively large in the stratified estuary ($R^*_{iE} \simeq 400$). In the partially mixed estuary, where the modified estuarine Richardson number is about 30~85, the intrusion distance is a minimum and exhibits a similar tendency to that of Komatsu et al.'s experimental results.

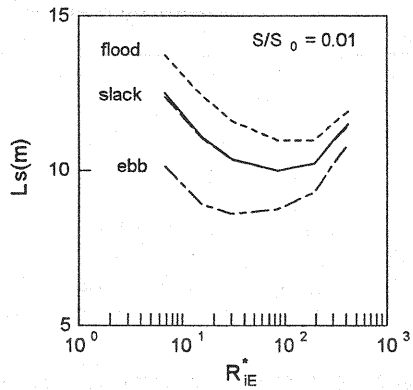

Fig.9 Salt intrusion distance as a function of modified estuarine Richardson number

Figure 10 shows the relationship between experiment and numerical values of intrusion distance. The agreement between experimental and computed results is highly satisfactory, excepting the partially mixed estuary with a tidal amplitude is 0.85 cm, where the computed results are slightly larger than the experimental ones.

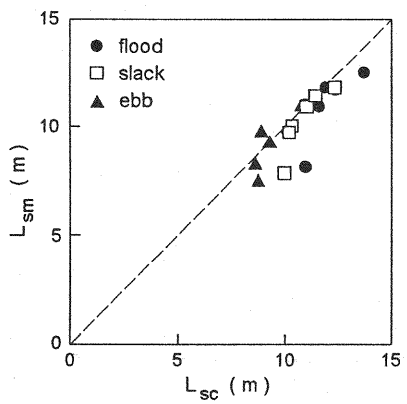

Fig.10 Comparison of intrusion distance (L_{sm} : experimental; L_{sc} : computed)

CONCLUSIONS

Using experiments conducted by Perrels-Karelse and Komatsu et al. for comparison, numerical analysis was carried out with temporal and spatial eddy viscosity and turbulent diffusivity. Simulated values for the vertical distribution of longitudinal velocity and salinity were satisfactory. However, this investigation has not yet reached a point which we can clarify the relationships between various parameters used in evaluating diffusivity and patterns of mixing, the characteristics of tide, and river water discharge. Further numerical analysis will be necessary for a quantitative evaluation of turbulent diffusivity.

ACKNOWLEDGEMENT

This research was supported by the Science Research Fund of the Ministry of Education(representative : Hitoshi Tanaka).

REFERENCES

1. Bear J. : Hydraulics of Groundwater, McGraw-Hill, pp.225-239, 1979.
2. Ellison, T.H. and J.S.Turner : Turbulent entrainment in stratified flows, J.Fluid Mech., Vol.6, pp.423-448, 1960.
3. Fischer, H.B. : Mass transport mechanisms in partially stratified estuary, J.Fluid Mech., Vol.53, pp.671-687, 1972.
4. Fischer, H.B. : Mixing and dispersion in estuaries, Annual Review Fluid Mech., Vol.8, pp.107-133, 1976.
5. Komatsu, T., T.Adachi, S.Sun and T.Shibata : The method for evaluation of apparent dispersion flux in a well-mixed estuary, Ann.J.Hydraul.Eng., JSCE, Vol.40, pp.505-510, 1996.(in Japanese)
6. Perrels, P.A.J. and M.Karelse : A two-dimensional numerical model for salt intrusion in estuaries, in: J.C.J.Nihoul (editor), Hydrodynamics of Estuaries and Fjords, Elsevier Scientific Publishing Company, pp.107-125, 1978.
7. Smagorinsky, J. : General circulation experiments with primitive equations, Month Weather Rev., Vol.9, No.3, pp.99-164, 1963.

APPENDIX - NOTATION

The following symbols are used in this papaer;

a	= tidal amplitude;
a_T, a_L	= characteristic lengths defined by Eq.10;
B	= channel width;
c_1	= empirical constant;
c_s	= Smagorinsky constant;
f_b	= transfer coefficient as defined by Eq.17;
F_1, F_2, F_3	= transfer coefficients as defined by Eq.19;
g	= gravitational acceleration;
h	= still water depth;
K_{xx}, K_{zz}	= longitudinal and vertical turbulent diffusivities, respectively;
$\tilde{K}_{xx}$	= normalized longitudinal turbulent diffusivity
L_{sc}	= computed intrusion distance;
L_{sm}	= intrusion distance by Komatsu et al.'s experiment;
p	= pressure;
Q	= river water discharge at the upstream boundary;
R^*_{iE}	= modified estuarine Richardson number as defined by Eq.20;
s	= relative difference density ($s=(\rho_s-\rho_0)/\rho_0$);
S	= salinity;
S_0	= salinity of the sea;
t	= time;
T	= tidal period;
u, w	= longitudinal and vertical velocities, respectively;
u_ξ, w_ξ	= longitudinal and vertical velocities at the water surface, respectively;
u_*	= r.m.s. of shear velocity;
x, z	= longitudinal and vertical coordinates, respectively;
z_b	= z-coordinate of the bottom;
z'	= transformed coordinate as defined by Eq.17;
$\tilde{z}$	= height from the bottom;
γ_x, γ_z	= constants of proportionality;
Δx, Δz	= longitudinal and vertical grid intervals, respectively;
ζ	= water level;
η	= surface elevation;
ν, ν_t	= kinematic viscosity and SGS diffusivity;
ξ	= position of the free water surface;
ρ	= fluid density
ρ_0, ρ_s	= density of fresh and salt waters, respectively;
σ	= angular frequency; and
τ_{xx}, τ_{zx}	= Reynolds stresses.

(Received August 21,1998 ; revised November 6, 1998)